Title

Determination of location, size, and transmurality of chronic myocardial infarction without exogenous contrast media by using cardiac magnetic resonance imaging at 3 T.

Journal
Circulation. Cardiovascular imaging, 7(3)

ISSN
1941-9651

Authors
Kali, Avinash
Cokic, Ivan
Tang, Richard LQ
et al.

Publication Date
2014-05-01

DOI
10.1161/circimaging.113.001541

Peer reviewed

Published in final edited form as:
Circ Cardiovasc Imaging. 2014 May ; 7(3): 471–481. doi:10.1161/CIRCIMAGING.113.001541.

Determination of Location, Size and Transmurality of Chronic Myocardial Infarction Without Exogenous Contrast Media Using Cardiac Magnetic Resonance Imaging at 3T

Avinash Kali, MS[1,2,3], **Ivan Cokic, MD**[1], **Richard L Q Tang, MD**[1,3], **Hsin-Jung Yang, MS**[1,2], **Behzad Sharif, PhD**[1], **Eduardo Marbán, MD, PhD**[4], **Debiao Li, PhD**[1,3,4], **Daniel Berman, MD**[4,5], and **Rohan Dharmakumar, PhD**[1,3,4,5]

[1]Biomedical Imaging Research Institute, Department of Biomedical Sciences, Cedars-Sinai Medical Center, Los Angeles, CA

[2]Department of Bioengineering, University of California, Los Angeles, CA

[3]Department of Radiology, Northwestern University, Chicago IL

[4]Cedars-Sinai Heart Institute, Cedars-Sinai Medical Center, Los Angeles CA

[5]Department of Medicine, David Geffen School of Medicine, University of California, Los Angeles, CA

Abstract

Background—LGE CMR is a powerful method for characterizing MI, but the requisite gadolinium infusion is estimated to be contraindicated in nearly 20% of MI patients due to end-stage chronic kidney disease. The purpose of this study is to investigate whether T_1 Cardiovascular-Magnetic-Resonance Imaging (CMR) obtained without contrast agents at 3T could be an alternative to Late-Gadolinium-Enhanced (LGE) CMR for characterizing chronic myocardial infarctions (MIs) using a canine model of MI.

Methods and Results—Canines (n=29) underwent CMR at 7 days (acute, AMI) and 4 months (chronic, CMI) post-MI. Infarct location, size and transmurality measured using native T_1 maps and LGE images at 1.5T and 3T were compared. Resolution of edema between AMI and CMI was examined with T_2 maps. T_1 maps overestimated infarct size and transmurality relative to LGE images in AMI ($p=0.016$ and $p=0.007$, respectively), which was not observed in CMI ($p=0.49$ and $p=0.81$, respectively), at 3T. T_1 maps underestimated infarct size and transmurality relative to LGE images in AMI and CMI ($p<0.001$), at 1.5T. Relative to the remote territories, T_1 of the infarcted myocardium was increased in CMI and AMI ($p<0.05$); and T_2 of the infarcted myocardium was increased in AMI ($p<0.001$), but not in CMI ($p>0.20$) at both field strengths. Histology showed extensive replacement fibrosis within the CMI territories. CMI detection sensitivity and specificity of T_1 CMR at 3T were 95% and 97%, respectively.

Correspondence to: Rohan Dharmakumar, PhD, Dept of Biomedical Sciences, Cedars-Sinai Medical Center, Biomedical Imaging Research Institute, PACT Bldg – Suite 800; 8700 Beverly Blvd, Los Angeles, CA 90048, Phone: (310) 423-7641, Fax: (310) 248-8682, rohandkumar@csmc.edu.

Disclosures
None.

Conclusions—Native T_1 maps at 3T can determine the location, size and transmurality of CMI with high diagnostic accuracy. Patient studies are necessary for clinical translation.

Keywords

myocardial infarction; viability imaging; fibrosis; T_1 mapping

Prognostic outcome in patients with myocardial infarction (MI) is significantly determined by the location, size and transmurality of the MI[1–5]. Over the past decade, Late Gadolinium Enhancement (LGE) Cardiac Magnetic Resonance Imaging (CMR) has evolved into a robust non-invasive imaging technique for detecting acute MIs (AMI) and chronic MIs (CMI) with excellent diagnostic accuracy and prognostic significance[6–8]. However, accurate infarct sizing using LGE imaging is limited by the gadolinium kinetics[9–11], effective nulling of the remote myocardium[12], and its qualitative nature. Contrast-enhanced T_1 mapping has been proposed as a potential alternative as it is quantitative in nature, and does not require nulling of the remote myocardium[13, 14]. Nevertheless, like LGE imaging, the T_1 value of infarcted myocardium in contrast-enhanced T_1 mapping depends on the gadolinium kinetics[15]. Moreover, once contrast-enhanced imaging is deemed necessary for assessment of myocardial viability, all other imaging sequences are typically required to be prescribed ahead of LGE imaging, which could impose practical limitations on the execution of the imaging exam, especially when rapid assessment of viability is all that may be necessary. Finally, perhaps most importantly, contrast-enhanced imaging requires administration of a gadolinium chelate, which is contraindicated in patients with chronic end-stage kidney disease[16], which is a rising epidemic[17]. In fact, according to the Unites States Renal Data System, the fraction of patient with cardiovascular disease, who have chronic kidney disease is >40%. Recent studies have shown that approximately 20% of AMI (STEMI and NSTEMI) patients suffer from late stage chronic kidney disease (GFR <45 mL/min/1.73m^2), in whom LGE is expected to be contraindicated[18, 19].

By definition, native T_1 mapping does not require exogenous contrast media. Hence in addition to the patients with renal insufficiency, the technique can be safely used in significant fraction of patients for whom LGE imaging or contrast-enhanced T_1 mapping is warranted but are contraindicated for gadolinium. Recent studies have shown that native T_1 mapping can reliably detect AMI at both 1.5T and 3T[13, 20–22]. In contrast, the diagnostic performance of native T_1 mapping to detect CMI has been shown to be poor at 1.5T[13]. Preliminary studies in non-ischemic cardiac pathologies in animals and humans have noted intrinsic T_1 dependence on myocardial collagen content[23]. Recent studies have demonstrated the tremendous potential of native T_1 mapping at 3T to reliably detect and quantify diffuse myocardial fibrosis in non-ischemic settings, such as aortic stenosis[24], hypertrophic cardiomyopathy[25, 26] and dilated cardiomyopathy[25, 26].

We hypothesized that magnetic field dependent T_1 elongations permit native T_1 mapping to reliably detect and quantify replacement myocardial fibrosis associated with CMI at 3T. To test our hypothesis, we rigorously studied the native T_1 characteristics against LGE features of myocardial images acquired at 1.5T and 3T using canine models of AMI and CMI.

Methods

Animal Model

Canines (n = 33; 20–25 kg body weight) were studied according to the protocols approved by Institutional Animal Care and Use Committees. Myocardial infarction was created by ligating the left anterior descending (LAD) artery for 3 hours followed by reperfusion. Animals were allowed to recover for 7 days before the Cardiac Magnetic Resonance (CMR) studies.

Cardiac Magnetic Resonance Studies

Four canines died during the first few hours of reperfusion despite resuscitation efforts. The remaining 29 canines underwent CMR studies at 7 days (acute) and 4 months (chronic) following reperfusion. Nineteen of the 29 canines were scanned on a 3T clinical MRI system (MAGNETOM Verio®, Siemens Healthcare, Erlangen, Germany), while the remaining ten canines were scanned on a 1.5T clinical MRI system (MAGNETOM Espree®, Siemens Healthcare, Erlangen, Germany). ECG-triggered breath-held cine-SSFP, native T_1-weighted and T_2-weighted images of contiguous slices covering the entire LV were acquired along the short-axis views at both 3T and 1.5T. All imaging studies were completed with the acquisition of Late Gadolinium Enhancement (LGE) images 8–10 minutes following intravenous administration of 0.2 mmol/kg gadopentate dimeglumine (Magnevist, Bayer Healthcare Pharmaceuticals Inc., Wayne, NJ). Imaging sequences and measurement parameters used to acquire the various images are summarized in Table 1. To minimize surface coil bias, pre-scan normalization was applied for each scan.

Histopathology

All animals were euthanized following the 4-month CMR study and their hearts were excised. Ex-vivo triphenyl tetrazolium chloride (TTC) staining and Elastin Masson’s Trichrome (EMT) staining were performed.

Image Analyses

T_1 and T_2 maps were constructed from the native T_1-weighted and T_2-weighted images, respectively. All image analyses were performed on cvi42 image analysis software (Circle Cardiovascular Imaging Inc., Calgary, Canada). Remote (viable) myocardium was identified on LGE images as the region showing no hyperintensity and a reference ROI was drawn in it. Infarcted myocardium was identified on the LGE image as the region with mean signal intensity (SI) >5 standard deviations (SDs) than that of reference ROI[27–29]. Hypointense cores of microvascular obstruction that were not detected as infarcted myocardium on LGE images by the thresholding criterion were manually included in the final analysis for infarct size and transmurality. The reference ROI drawn on LGE image was copied on to the corresponding T_1 map. Infarcted myocardium was then identified on the T_1 map using the mean+5SD criterion. To account for the dependence of MOLLI T_1 values on heart rate, the T_1 values were corrected and the threshold was further adjusted as previously described[13]. Hypointense cores of acute hemorrhage or chronic iron deposition[30, 31] that were not detected as infarcted myocardium on T_1 maps by the thresholding criterion were manually included in the final analysis for infarct size and transmurality.

Infarct sizes from both LGE images and T_1 maps were measured as the percentage of total left-ventricular (LV) volume, as well as on the basis of standard American Heart Association (AHA) 17-segment model. Measurements from the 17th segment were excluded from the final analysis to discount the partial volume effects at the apical cap. Infarct transmurality was determined as the percentage extent of the infarct along 100 equally spaced chords on each slice. Mean transmurality was obtained by averaging the infarct transmurality across all the chords that have at least 1% scar extent.

T_1 and T_2 values of the remote and infarcted myocardium (as identified on LGE images using mean+5SD criterion) were measured from T_1 and T_2 maps respectively. Hypointense cores within infarcted myocardium were excluded from this analysis to eliminate the confounding effects of acute hemorrhage or chronic iron deposition on acute myocardial edema or chronic replacement fibrosis

Statistical Analyses

Statistical analyses were performed using IBM SPSS Statistics (version 21.0, IBM Corporation, Armonk, New York). Normality of the data was tested using the Shapiro-Wilk test and quantile-quantile plots. Depending on the normality of the data, percentage infarct size and mean transmurality measured over the entire LV were compared between LGE images and T_1 maps using either paired t-test or Wilcoxon signed-rank test. Additionally, mixed-model ANOVA was used to compare percentage segmental infarct size measured from the two techniques. Bland-Altman analysis was performed to estimate the agreement between the two techniques. Simple linear regression was performed to estimate the correlation between the two techniques with respect to infarct size and transmurality measurements. Measurements from the native T_1 maps and LGE images were chosen as the dependent and explanatory variables respectively. The slope and the intercept of the best fit line were tested to be equal to 1 and 0 respectively. Using LGE images as the gold standard, sensitivity and specificity of native T_1 maps to detect infarcted myocardium at the segmental level were measured. Receiver operating characteristic (ROC) analysis was performed to measure area under the curve (AUC). The predictor variable used to generate the ROC curves was the infarct size measured on a segmental basis from the T_1 maps.

T_1 and T_2 values of the remote and infarcted myocardium were compared using mixed-model ANOVA. Similarly, percentage change in the LGE-SI of infarcted myocardium relative to remote myocardium was compared to the percentage change in T_1. Statistical significance was set at $p<0.05$ for all analyses.

Results

Detection of Acute Myocardial Infarction at 3T

All canines sustained MIs as verified by the presence of gadolinium hyperenhancement on LGE images acquired at 7 days post-reperfusion. Representative LGE images and T_1 maps acquired at 7 days post-MI from a canine scanned at 3T are shown in Figure 1. Bulls-eye plots depicting the infarct extent on 17-segment model and transmurality are also shown for both LGE images and T_1 maps in Figure 1. Infarct location and spatial extent were visually well correlated between LGE images and T_1 maps. In AMI at 3T, T_1 maps modestly overestimated infarct size (13.3±8.4% vs. 11.6±6.8%, p=0.007) and transmurality (64±19% vs. 56±17%, p=0.007) relative to LGE images. Mean segmental infarct size measured using T_1 maps was also greater than that measured using LGE images (p=0.016). Bland-Altman analysis showed good agreement between LGE images and T_1 maps for measuring infarct size (Bias = 2.22±2.34%; Figure 2A) and transmurality (Bias = 7.07±10.25%; Figure 2B). Strong correlations were observed between LGE images and T_1 maps for measuring infarct size (R^2=0.94; Slope=1.20, p=0.011; Intercept=0.01, p=0.98; Figure 2C) and transmurality (R^2=0.72; Slope=0.93, p=0.62; Intercept=11.14; p=0.20; Figure 2D). At 3T, T_1 maps detected AMI in 149 of 158 segments that were positive for infarction on LGE images (94% sensitivity; 95% confidence interval (CI): 90–98). T_1 maps were negative for AMI in 138 of 146 segments (94% specificity; 95% CI: 91–98). ROC analysis showed that the area under the curve was 0.96 (Figure 2E).

Detection of Chronic Myocardial Infarction at 3T

Representative LGE images and T_1 maps, along with the bulls-eye plots for infarct extent and transmurality, acquired from a canine scanned at 3T at 4 months post MI are shown in Figure 3. Infarct locations and its spatial extent were visually identical on LGE images and T_1 maps in CMI. There was no significant difference between the LGE images and T_1 maps for measuring infarct size (5.6±3.7% vs. 5.5±3.7%; p=0.61) and transmurality (44±15% vs. 46±15%; p=0.81). Mean segmental infarct size, measured using T_1 maps, was not different compared to that measured using LGE images (p=0.49). Bland-Altman analysis showed excellent agreement between LGE images and T_1 maps for measuring infarct size (Bias = −0.08±0.68%; Figure 4A) and transmurality (Bias = 0.45±8.14%; Figure 4B). Excellent correlations were observed between LGE images and T_1 maps for measuring infarct size (R^2=0.97; Slope=0.98, p=0.68; Intercept=0.02, p=0.94; Figure 4C) and transmurality (R^2=0.75; Slope=0.84, p=0.18; Intercept=8.11, p=0.18; Figure 4D). At 3T, T_1 maps detected CMI in 135 of 142 segments that were positive for infarction on LGE images (95% sensitivity; 95% CI: 92–99). T_1 maps were negative for CMI in 158 of 162 segments (97% specificity; 95% CI: 95–100). ROC analysis showed that the area under the curve was 0.99 (Figure 4E).

Detecting Acute Myocardial Infarction at 1.5T

Representative LGE images and T_1 maps, along with bulls-eye plots (obtained using the mean+5SD criterion), acquired from a canine scanned at 1.5T at 7 days post MI are shown in Supplementary Figure 1. Infarct location was visually well correlated between LGE images and T_1 maps at 1.5T. However, using the mean+5SD criterion at 1.5T, T_1 maps significantly underestimated the infarct size (9.4±5.6% vs. 15.5±9.4%, respectively, p<0.001) and transmurality (59±5% vs. 76±6%, respectively, p<0.001) in AMI relative to LGE images. Segmental comparison of infarct sizes also showed significant underestimation by T_1 maps compared to LGE images (p<0.001). Bland-Altman analysis showed moderate agreement between LGE images and T_1 maps for measuring infarct size (Bias = −8.07±4.6%; Figure 5A) and transmurality (Bias = −17.61 ±3.27%; Figure 5B) measured using the mean+5SD criterion. However, strong correlations were observed between LGE images and T_1 maps for measuring acute infarct size (R^2=0.86; Slope=0.57, p<0.001; Intercept = −1.40, p=0.36; Figure 5C) and transmurality (R^2=0.77; Slope=0.71, p=0.06; Intercept=4.63, p=0.66; Figure 5D). At 1.5T, T_1 maps were positive for AMI in 92 of 110 segments (84% sensitivity; 95% CI: 77–91), and negative for AMI in 37 of 50 segments (74% specificity; 95% CI: 62–86). ROC analysis showed that the area under the curve was 0.86 (Figure 5E). Using the previously reported mean+3SD criterion[13] for detecting AMI on T_1 maps at 1.5T, infarct size (16.4±8.2%) and transmurality (81±9%) measured using T_1 maps were not significantly different from those measured using the mean+5SD criterion on LGE images (p=0.28 for infarct size and p=0.18 for transmurality).

Detecting Chronic Myocardial Infarction at 1.5T

Representative LGE images and T_1 maps, along with bulls-eye plots (obtained using the mean+5SD criterion), acquired from a canine scanned at 1.5T at 4 months post-MI are shown in Supplementary Figure 2. Mean infarct size (2.1±1.2% vs. 4.8±1.8%, p<0.001) and transmurality (47±7% vs. 66±9%, p<0.001) measured on T_1 maps using the mean+5SD criterion in CMI were significantly lower than those measured on LGE images. Segmental comparison of infarct sizes in CMI showed significant underestimation by T_1 maps compared to LGE images (p<0.001). Bland-Altman analysis showed poor agreement between LGE images and T_1 maps for measuring infarct size (Bias = −2.74±1.31%; Figure 6A) and transmurality (Bias = −19.67±6.70%; Figure 6B). Moderate correlations were observed between LGE images and T_1 maps for measuring infarct size (R^2=0.44; Slope=0.43, p=0.004; Intercept= −0.03, p=0.97; Figure 6C) and transmurality (R^2=0.51; Slope=0.61, p=0.10; Intercept=6.60, p=0.65; Figure 6D). At 1.5T, T_1 maps were positive for CMI in 52 of 90 segments (58% sensitivity; 95% CI: 48–68), and negative for CMI in 55 of 70 segments (78% specificity; 95% CI: 69–88). ROC analysis showed that area under the curve was 0.79 (Figure 6E). Using the less stringent mean+3SD criterion for detecting CMI on T_1 maps at 1.5T, T_1 maps still significantly underestimated the infarct size and transmurality relative to those measured using mean+5SD criterion on LGE images (infarct size from T_1 map: 3.4±1.6%, p<0.001; transmurality from T_1 map: 52±20%, p<0.001).

T_1, T_2 and LGE Characteristics of Infarcted Myocardium at 3T and 1.5T in Acute and Chronic Infarctions

Table 2 summarizes the T_1, T_2 and LGE-SI characteristics of infarcted and remote myocardium at 3T and 1.5T at 7 days and 4 months post-MI. Representative LGE images, T_1 maps and T_2 maps acquired from four different canines at 3T and 1.5T during the acute and chronic phases of MI are shown in Figure 7.

Compared to remote myocardium, mean T_1 and T_2 of the infarcted myocardium were increased by 329± 119ms and 18±6ms respectively in AMI at 3T (p<0.001 for both cases). In terms of infarcted to remote myocardium contrast, percentage change in LGE-SI was nearly 28-fold higher than percentage change in T_1 (p<0.001). However, the coefficient of variation (CV) of the percentage change in LGE-SI was two-fold higher than percentage change in T_1 (0.66 vs. 0.30) indicating a greater variability in LGE versus T_1 image contrast.

In CMI, significant T_1 increase was still visually evident within infarcted myocardium at 3T, while edema within the infarcted myocardium, typically visualized via T_2 images, appeared to have resolved. Mean T_1 of infarcted myocardium in CMI at 3T was increased by 239±104ms with respect to remote myocardium (p<0.001), while mean difference in T_2 values of infarcted and remote myocardium in CMI at 3T was not statistically significant (2±3ms; p=0.19). Mean T_1 of the infarcted myocardium in CMI was significantly lower than that in AMI (p<0.001). However, no significant difference was observed between mean T_1 values of remote myocardium measured during the acute and chronic phases (p=0.21). Consistent with the acute studies, percentage change in LGE-SI was nearly 40-fold higher than percentage change in T_1 (p<0.001). However, the CV of percentage change in LGE-SI was 1.5-fold higher (0.65) compared to percentage change in T_1 (0.42), again indicating a higher degree of variability in LGE versus T_1 image contrast.

In AMIs at 1.5T, significant T_2 increase was visually evident within infarcted myocardium, while moderate T_1 increase was visible in infarcted myocardium. Mean T_1 of infarcted myocardium at 1.5T in AMI was 184±77ms higher than that of remote myocardium (p<0.001), while mean T_2 of infarcted myocardium was 20±7ms higher than that of remote myocardium (p<0.001). Percentage change in the LGE-SI was nearly 26-fold higher than percentage change in T_1 at 1.5T (p<0.001). Compared to 1.5T, infarcted to remote myocardium T_1 contrast in AMI was nearly 2-fold higher at 3T.

After 4 months post-MI, neither T_1 nor T_2 increase was visually evident within infarcted myocardium at 1.5T. Mean T_1 value of infarcted myocardium at 1.5T in CMI was mildly higher by 89±38ms than that of remote myocardium (p=0.037). Mean difference in T_2 values of infarcted and remote myocardium was not statistically different from 0 (2±5ms; p=0.55). Mean T_1 of the infarcted myocardium in CMI was significantly lower than that in AMI (p<0.001). No significant difference was observed between the mean T_1 values of the remote myocardium during the acute and chronic period of MI (p=0.23). Percentage change in the LGE-SI was 34-fold higher than percentage change in T_1 at 1.5T (p<0.001). Compared to 1.5T, infarcted to remote myocardium T_1 contrast in CMI was nearly 50% higher at 3T.

Histopathological Validation of Replacement Fibrosis in CMI

Figure 8 shows representative LGE images and T_1 maps acquired at 3T from three different canines at 4 months post-reperfusion along with slice-matched ex-vivo TTC and EMT staining images. Both LGE images and T_1 maps agreed well with ex-vivo TTC images in terms of the spatial location of the infarction. EMT staining showed extensive replacement fibrosis within infarcted myocardium, which validated that T_1 hyperintensity in the CMI predominantly arose from fibrosis. Similar evidence was observed in the other animals.

Discussion

Characterizing CMIs using CMR has immense clinical importance for predicting long-term LV function[3], assessing the efficacy of therapeutic regeneration[32, 33] and risk stratifying patients for cardiac defibrillator implantation[34]. However, the utility of LGE imaging for this purpose is partly limited by the contra-indication of gadolinium infusion in nearly 20%

of the patients with AMI with chronic end-stage kidney disease[17–19]. Non-contrast approaches for viability imaging can, therefore, be of significant value for the clinical and therapeutic management of patients with MI.

Our study confirms the hypothesis that native T_1 mapping at 3T can reliably characterize CMIs with high specificity and sensitivity. Using a canine model of MIs and threshold-based detection of infarcted myocardium, we have demonstrated that native T_1 maps at 3T can accurately determine location, size and transmurality of CMI just as well as LGE CMR. We also found that using the same threshold-based criterion on native T_1 maps at 1.5T tended to significantly underestimate infarct size and transmurality obtained from LGE images in both AMI and CMI. We also tested whether using the previously tested, less stringent, mean+3SD criterion[13] significantly improves the diagnostic performance of T_1 mapping at 1.5T. Consistent with the previously reported observations, our results indicated that T_1 maps at 1.5T can reliably determine infarct size using the mean+3SD criterion in AMI[13], but significantly underestimates infarct size at 1.5T in the CMI despite the less stringent criteria. The ability to reliably detect infarcted myocardium at 3T compared to 1.5T is further explained by our findings that infarcted to remote myocardium T_1 contrast is 2-fold higher at 3T relative to 1.5T in AMI, and 1.5-fold higher in CMI. Our results suggested that native T_1 mapping at 3T can be a reliable alternative to LGE for characterizing CMI with the potential for clinical translation. In addition, our results are consistent with previously reported observations that myocardial edema, as detected using T_2-based imaging, resolves in the chronic phase of infarction[35, 36], and T_2-based imaging in conjunction with LGE imaging can be used to differentiate between AMIs and CMIs[37]. Hence, together with T_2 and T_1 maps it may be possible to reliably discriminate CMI in much the same way T_2 imaging is used for discriminating CMI when LGE is available.

LGE imaging and contrast-enhanced T_1 mapping are primarily limited by the association of gadolinium use to nephrogenic systemic fibrosis in patients with late-stage chronic kidney disease[38, 39]. Further, as observed from the high CV in the LGE contrast in our study, gadolinium kinetics in infarcted and remote myocardium lead to dynamic changes in LGE-SI values and contrast-enhanced T_1 values which may be irreproducible across different imaging sessions. These limitations may be overcome by the application of contrast-free techniques for assessing myocardial infarctions. Recently, $T_{1\rho}$ imaging was proposed as a potential contrast-free CMR technique for detecting AMI[40] and CMI[41]. However, this technique is limited by its high specific absorption rate (SAR), which can further limit the contrast between infarcted and remote myocardium. Native T_1 mapping overcomes many of the limitations faced by other techniques and opens the door to unique opportunities. First, it enables infarct characterization in patients with poor renal function, and is not SAR-limited. Second, it can improve the work flow demands during imaging exams: (a) allows for infarct characterization typically performed with LGE to be executed in any order within the imaging session, (b) eliminates the need to determine the inversion time, which continually changes as a function of the wash-out kinetics of the gadolinium-based contrast media, and (c) removes the waiting period between contrast administration and LGE acquisitions. Third, since pixel intensities of T_1 maps provide intrinsic T_1 values, it makes the approach inherently quantitative, which permits reliable serial examinations of infarct healing and remodeling, especially when prescribed with a T_1 mapping approach that is less sensitive to heart rate variations[20]. Finally, it can render significant cost savings since contrast infusions and venous cannulations would become unnecessary and the length of the imaging exam may be reduced.

Previous studies have reported that myocardial edema associated with AMI can be accurately detected and sized using T_1-weighted imaging[42] and native T_1 maps at both 1.5T and 3T[13, 20–22]. Consistently, our study showed that T_1 elevation in AMI is accompanied by T_2 elevation, indicating that the ability of T_1 mapping to reliably detect AMI predominantly arose from increased free water content in infarcted myocardium[21, 37]. Although the clinical value of native T_1 maps for detecting AMI has been well studied, its potential for assessing CMI has not been fully explored to date. Messroghli et al[13] and Bauner et al[14] have shown that, at 1.5T, CMIs are associated with significant increase in native T_1. However, the diagnostic performance of native T_1 maps at 1.5T to detect CMI has been reported to be poor. Recently, Dall'Armellina and colleagues have reported preliminary case studies at 3T in which T_1 hyperenhancement could be observed even in CMI without any concomitant T_2 increase[43]. However, the nature of such T_1 hyperenhancement was not fully elucidated. This study showed that that the extensive replacement fibrosis associated with CMI might be responsible for the observed T_1 elevations in chronic phase of MI. The reversion of T_2 values of infarcted myocardium to baseline levels, which indicates complete resolution of edema[37], additionally support the notion that the apparent T_1 elevations in CMI may be predominantly due to fibrosis. This is consistent with previous reports showing significant T_1 elevations associated with diffuse myocardial fibrosis in non-ischemic cardiomyopathies such as aortic stenosis[24], hypertrophic cardiomyopathy[25, 26] and idiopathic dilated cardiomyopathy[25, 26].

Our study showed that one of the primary reasons that CMIs are more reliably characterized at 3T is due to the biophysical differences in T_1 relaxation of remote myocardium and infarcted myocardium at 3T and 1.5T. We found that, as the field strength is increased from 1.5T to 3T, the T_1 values of the non-infarcted (remote) myocardium and the infarcted (fibrotic) myocardium are increased by ~ 29% and ~ 40% (Table 2), respectively. This is consistent with previous studies, which have rigorously shown that T_1 of a given tissue can increase between ~10% to ~70% at 3T compared to 1.5T, and that the extent of the increase is dependent on the type of tissue[44]. Although the mechanistic underpinnings of native T_1 elongation in CMIs are not entirely clear, there are a few possible explanations. One potential mechanism is that the apparent diffusion coefficient in CMIs is higher than that of remote myocardium[45, 46], which implies greater diffusivity of water molecules, lower viscosity, lower correlation times of molecular motion and hence longer T_1 values[47]. In addition, another possibility is the potential bias in T_1 values measured using MOLLI sequences with SSFP readouts which may be subject to magnetization transfer (MT) effects. Robson et al have shown that MT effects can lead to T_1 underestimation by MOLLI[48]. Scholz et al[49] and Weber et al[50] have shown that the MT effects are reduced in AMIs and CMIs, which could potentially lead to longer apparent T_1 values within infarcted myocardium. Nevertheless, further studies are necessary to fully elucidate the mechanisms and their relative contributions to the underlying T_1 elongations observed in CMIs.

Our study showed that LGE images have a nearly 30-fold higher infarcted to remote myocardium contrast relative to the proposed native T_1 maps at 3T. While the high image contrast of infarcted myocardium in LGE images is attributable to the use gadolinium-based contrast agents, the imposed nulling of remote myocardium by inversion-recovery preparation is another significant contributor to the observed contrast. In this context, it should be noted that as in LGE imaging, inversion-recovery preparation may also be introduced to significantly improve image contrast between infarcted and remote myocardium in native T_1-weighted techniques as well. Based on the T_1 values of remote myocardium (1250 ms) and CMIs (1490 ms) at 3T, an inversion-recovery preparation that nulls remote myocardium gives a 12% equilibrium magnetization available for readout from infarcted myocardium. Similarly, assuming that the contrast-enhanced T_1 values (10 minutes post-gadolinium injection) of remote and infarcted myocardium at 3T are 400 ms and 230 ms respectively, an inversion-recovery sequence that nulls remote myocardium (such as conventional LGE imaging) gives a 40% equilibrium magnetization available for readout from infarcted myocardium. This suggests that, if employed, inversion-recovery preparation can potentially increase the image contrast between infarcted and remote myocardium by 900% compared to the current levels. Experimental studies are necessary to confirm these theoretical estimations. Nevertheless, while this is expected to improve the visualization of CMI, the current T_1 mapping approach evaluated here still provides excellent diagnostic accuracy.

Together with previous studies, our study has shown that native T_1 mapping has great potential for widespread clinical applicability in the setting CMI. While a few studies have assessed the prognostic significance of T_1 hyperenhancement in AMI[21, 22], future studies that elucidate the relationship of T_1 hyperenhancement in the CMI to long-term LV function, collagen metabolism and extracellular matrix remodeling are necessary.

Study Limitations

First, the sample size used in this study is relatively small, but comparable to those used in previous studies in patients with MIs[13, 14, 21, 22]. Second, this study relied on identifying the remote territory on the basis of LGE. Additional studies are necessary to examine whether remote territories can be reliably identified solely on the basis of native T_1 maps. Third, we did not evaluate the proposed approach in the clinical setting. Hence, additional studies are required to determine the diagnostic performance of native T_1 maps in patients with CMI. Third, we limited our analysis to the mean+5SD threshold as this criterion has been shown to be robust for delineating infarcted myocardium in LGE imaging[27–29]. Nevertheless, a comprehensive study comparing the different thresholding criteria to ex-vivo histology-based infarct sizing may be necessary for further validation. However, such a study needs to take into account potential changes in T_1 following animal sacrifice and registration between CMR images and ex-vivo standard. Finally, our analysis was limited to LAD infarctions. Additional studies are needed to extend our findings to infarctions in other coronary territories.

Conclusion

Native T_1 mapping at 3T can reliably determine infarct location, size, and transmurality of CMI with high diagnostic accuracy that is comparable to conventional LGE imaging. Given its non-reliance on exogenous contrast media, potential efficiency improvements associated with workflow during imaging sessions, and quantitative nature, native T_1 mapping provides an appealing alternative for viability imaging when LGE imaging is contraindicated. Patient studies are necessary for clinical translation.

Supplementary Material

Refer to Web version on PubMed Central for supplementary material.

Acknowledgments

Sources of Funding

This work was supported in part by grants from American Heart Association (13PRE17210049) and National Heart, Lung, And Blood Institute (HL091989).

References

1. Pfeffer MA, Braunwald E. Ventricular remodeling after myocardial infarction. Experimental observations and clinical implications. Circulation. 1990; 81:1161–1172. [PubMed: 2138525]
2. Sutton MG, Sharpe N. Left ventricular remodeling after myocardial infarction: Pathophysiology and therapy. Circulation. 2000; 101:2981–2988. [PubMed: 10869273]
3. Orn S, Manhenke C, Anand IS, Squire I, Nagel E, Edvardsen T, Dickstein K. Effect of left ventricular scar size, location, and transmurality on left ventricular remodeling with healed myocardial infarction. Am J Cardiol. 2007; 99:1109–1114. [PubMed: 17437737]
4. Wu E, Ortiz JT, Tejedor P, Lee DC, Bucciarelli-Ducci C, Kansal P, Carr JC, Holly TA, Lloyd-Jones D, Klocke FJ, Bonow RO. Infarct size by contrast enhanced cardiac magnetic resonance is a stronger predictor of outcomes than left ventricular ejection fraction or end-systolic volume index: Prospective cohort study. Heart. 2008; 94:730–736. [PubMed: 18070953]
5. Kwon DH, Halley CM, Carrigan TP, Zysek V, Popovic ZB, Setser R, Schoenhagen P, Starling RC, Flamm SD, Desai MY. Extent of left ventricular scar predicts outcomes in ischemic cardiomyopathy patients with significantly reduced systolic function: A delayed hyperenhancement cardiac magnetic resonance study. JACC Cardiovasc Imaging. 2009; 2:34–44. [PubMed: 19356530]
6. Kim RJ, Fieno DS, Parrish TB, Harris K, Chen EL, Simonetti O, Bundy J, Finn JP, Klocke FJ, Judd RM. Relationship of MRI delayed contrast enhancement to irreversible injury, infarct age, and contractile function. Circulation. 1999; 100:1992–2002. [PubMed: 10556226]
7. Kim RJ, Wu E, Rafael A, Chen EL, Parker MA, Simonetti O, Klocke FJ, Bonow RO, Judd RM. The use of contrast-enhanced magnetic resonance imaging to identify reversible myocardial dysfunction. N Engl J Med. 2000; 343:1445–1453. [PubMed: 11078769]
8. Pennell DJ, Sechtem UP, Higgins CB, Manning WJ, Pohost GM, Rademakers FE, van Rossum AC, Shaw LJ, Yucel EK. Clinical indications for cardiovascular magnetic resonance (CMR): Consensus panel report. J Cardiovasc Magn Reson. 2004; 6:727–765. [PubMed: 15646878]
9. Knowles BR, Batchelor PG, Parish V, Ginks M, Plein S, Razavi R, Schaeffter T. Pharmacokinetic modeling of delayed gadolinium enhancement in the myocardium. Magn Reson Med. 2008; 60:1524–1530. [PubMed: 19025896]
10. Oshinski JN, Yang Z, Jones JR, Mata JF, French BA. Imaging time after Gd-DTPA injection is critical in using delayed enhancement to determine infarct size accurately with magnetic resonance imaging. Circulation. 2001; 104:2838–2842. [PubMed: 11733404]

11. Grebe O, Paetsch I, Kestler HA, Herkommer B, Schnackenburg B, Hombach V, Fleck E, Nagel E. Optimal acquisition parameters for contrast enhanced magnetic resonance imaging after chronic myocardial infarction. J Cardiovasc Magn Reson. 2003; 5:575–587. [PubMed: 14664135]
12. Kim RJ, Shah DJ, Judd RM. How we perform delayed enhancement imaging. J Cardiovasc Magn Reson. 2003; 5:505–514. [PubMed: 12882082]
13. Messroghli DR, Walters K, Plein S, Sparrow P, Friedrich MG, Ridgway JP, Sivananthan MU. Myocardial T1 mapping: Application to patients with acute and chronic myocardial infarction. Magn Reson Med. 2007; 58:34–40. [PubMed: 17659622]
14. Bauner KU, Biffar A, Theisen D, Greiser A, Zech CJ, Nguyen ET, Reiser MF, Wintersperger BJ. Extracellular volume fractions in chronic myocardial infarction. Invest Radiol. 2012; 47:538–545. [PubMed: 22836311]
15. Gai N, Turkbey EB, Nazarian S, van der Geest RJ, Liu CY, Lima JA, Bluemke DA. T1 mapping of the gadolinium-enhanced myocardium: Adjustment for factors affecting interpatient comparison. Magn Reson Med. 2011; 65:1407–1415. [PubMed: 21500267]
16. Ledneva E, Karie S, Launay-Vacher V, Janus N, Deray G. Renal safety of gadolinium-based contrast media in patients with chronic renal insufficiency. Radiology. 2009; 250:618–628. [PubMed: 19244037]
17. Puntmann VO, Gebker R, Duckett S, Mirelis J, Schnackenburg B, Graefe M, Razavi R, Fleck E, Nagel E. Left ventricular chamber dimensions and wall thickness by cardiovascular magnetic resonance: Comparison with transthoracic echocardiography. Eur Heart J Cardiovasc Imaging. 2013; 14:240–246. [PubMed: 22815376]
18. Fox CS, Muntner P, Chen AY, Alexander KP, Roe MT, Cannon CP, Saucedo JF, Kontos MC, Wiviott SD. Use of evidence-based therapies in short-term outcomes of ST-segment elevation myocardial infarction and non-ST-segment elevation myocardial infarction in patients with chronic kidney disease: A report from the national cardiovascular data acute coronary treatment and intervention outcomes network registry. Circulation. 2010; 121:357–365. [PubMed: 20065168]
19. Shroff GR, Frederick PD, Herzog CA. Renal failure and acute myocardial infarction: Clinical characteristics in patients with advanced chronic kidney disease, on dialysis, and without chronic kidney disease. A collaborative project of the United States Renal Data System/National Institutes of Health and the National Registry of Myocardial Infarction. Am Heart J. 2012; 163:399–406. [PubMed: 22424010]
20. Piechnik SK, Ferreira VM, Dall'Armellina E, Cochlin LE, Greiser A, Neubauer S, Robson MD. Shortened modified look-locker inversion recovery (ShMOLLI) for clinical myocardial T1-mapping at 1.5 and 3 T within a 9 heartbeat breathhold. J Cardiovasc Magn Reson. 2010; 12:69. [PubMed: 21092095]
21. Dall'Armellina E, Piechnik SK, Ferreira VM, Si QL, Robson MD, Francis JM, Cuculi F, Kharbanda RK, Banning AP, Choudhury RP, Karamitsos TD, Neubauer S. Cardiovascular magnetic resonance by non contrast T1-mapping allows assessment of severity of injury in acute myocardial infarction. J Cardiovasc Magn Reson. 2012; 14:15. [PubMed: 22309452]
22. Ferreira VM, Piechnik SK, Dall'Armellina E, Karamitsos TD, Francis JM, Choudhury RP, Friedrich MG, Robson MD, Neubauer S. Non-contrast T1-mapping detects acute myocardial edema with high diagnostic accuracy: A comparison to T2-weighted cardiovascular magnetic resonance. J Cardiovasc Magn Reson. 2012; 14:42. [PubMed: 22720998]
23. Grover-McKay M, Scholz TD, Burns TL, Skorton DJ. Myocardial collagen concentration and nuclear magnetic resonance relaxation times in the spontaneously hypertensive rat. Invest Radiol. 1991; 26:227–232. [PubMed: 1829067]
24. Bull S, White SK, Piechnik SK, Flett AS, Ferreira VM, Loudon M, Francis JM, Karamitsos TD, Prendergast BD, Robson MD, Neubauer S, Moon JC, Myerson SG. Human non-contrast T1 values and correlation with histology in diffuse fibrosis. Heart. 2013; 99:932–937. [PubMed: 23349348]
25. Dass S, Suttie JJ, Piechnik SK, Ferreira VM, Holloway CJ, Banerjee R, Mahmod M, Cochlin L, Karamitsos TD, Robson MD, Watkins H, Neubauer S. Myocardial tissue characterization using magnetic resonance noncontrast T1 mapping in hypertrophic and dilated cardiomyopathy. Circ Cardiovasc Imaging. 2012; 5:726–733. [PubMed: 23071146]

26. Puntmann VO, Voigt T, Chen Z, Mayr M, Karim R, Rhode K, Pastor A, Carr-White G, Razavi R, Schaeffter T, Nagel E. Native T1 mapping in differentiation of normal myocardium from diffuse disease in hypertrophic and dilated cardiomyopathy. JACC Cardiovasc Imaging. 2013; 6:475–484. [PubMed: 23498674]
27. Bondarenko O, Beek AM, Hofman MB, Kuhl HP, Twisk JW, van Dockum WG, Visser CA, van Rossum AC. Standardizing the definition of hyperenhancement in the quantitative assessment of infarct size and myocardial viability using delayed contrast-enhanced CMR. J Cardiovasc Magn Reson. 2005; 7:481–485. [PubMed: 15881532]
28. Schulz-Menger J, Bluemke DA, Bremerich J, Flamm SD, Fogel MA, Friedrich MG, Kim RJ, von Knobelsdorff-Brenkenhoff F, Kramer CM, Pennell DJ, Plein S, Nagel E. Standardized image interpretation and post processing in cardiovascular magnetic resonance: Society for Cardiovascular Magnetic Resonance (SCMR) board of trustees task force on standardized post processing. J Cardiovasc Magn Reson. 2013; 15:35. [PubMed: 23634753]
29. Amado LC, Gerber BL, Gupta SN, Rettmann DW, Szarf G, Schock R, Nasir K, Kraitchman DL, Lima JA. Accurate and objective infarct sizing by contrast-enhanced magnetic resonance imaging in a canine myocardial infarction model. J Am Coll Cardiol. 2004; 44:2383–2389. [PubMed: 15607402]
30. Pedersen SF, Thrysoe SA, Robich MP, Paaske WP, Ringgaard S, Botker HE, Hansen ES, Kim WY. Assessment of intramyocardial hemorrhage by T1-weighted cardiovascular magnetic resonance in reperfused acute myocardial infarction. J Cardiovasc Magn Reson. 2012; 14:59. [PubMed: 22935462]
31. Kali A, Kumar A, Cokic I, Tang RL, Tsaftaris SA, Friedrich MG, Dharmakumar R. Chronic manifestation of postreperfusion intramyocardial hemorrhage as regional iron deposition: A cardiovascular magnetic resonance study with ex vivo validation. Circ Cardiovasc Imaging. 2013; 6:218–228. [PubMed: 23403335]
32. Makkar RR, Smith RR, Cheng K, Malliaras K, Thomson LE, Berman D, Czer LS, Marban L, Mendizabal A, Johnston PV, Russell SD, Schuleri KH, Lardo AC, Gerstenblith G, Marban E. Intracoronary cardiosphere-derived cells for heart regeneration after myocardial infarction (CADUCEUS): A prospective, randomised phase 1 trial. Lancet. 2012; 379:895–904. [PubMed: 22336189]
33. Malliaras K, Smith RR, Kanazawa H, Yee K, Seinfeld J, Tseliou E, Dawkins JF, Kreke M, Cheng K, Luthringer D, Ho CS, Blusztajn A, Valle I, Chowdhury S, Makkar RR, Dharmakumar R, Li D, Marban L, Marban E. Validation of contrast-enhanced MRI to monitor regenerative efficacy after cell therapy in a porcine model of convalescent myocardial infarction. Circulation. 2013; 128:2764–75. [PubMed: 24061088]
34. Klem I, Weinsaft JW, Bahnson TD, Hegland D, Kim HW, Hayes B, Parker MA, Judd RM, Kim RJ. Assessment of myocardial scarring improves risk stratification in patients evaluated for cardiac defibrillator implantation. J Am Coll Cardiol. 2012; 60:408–420. [PubMed: 22835669]
35. Dall'Armellina E, Karia N, Lindsay AC, Karamitsos TD, Ferreira V, Robson MD, Kellman P, Francis JM, Forfar C, Prendergast BD, Banning AP, Channon KM, Kharbanda RK, Neubauer S, Choudhury RP. Dynamic changes of edema and late gadolinium enhancement after acute myocardial infarction and their relationship to functional recovery and salvage index. Circ Cardiovasc Imaging. 2011; 4:228–236. [PubMed: 21447711]
36. Mather AN, Fairbairn TA, Artis NJ, Greenwood JP, Plein S. Timing of cardiovascular MR imaging after acute myocardial infarction: Effect on estimates of infarct characteristics and prediction of late ventricular remodeling. Radiology. 2011; 261:116–126. [PubMed: 21828188]
37. Abdel-Aty H, Zagrosek A, Schulz-Menger J, Taylor AJ, Messroghli D, Kumar A, Gross M, Dietz R, Friedrich MG. Delayed enhancement and T2-weighted cardiovascular magnetic resonance imaging differentiate acute from chronic myocardial infarction. Circulation. 2004; 109:2411–2416. [PubMed: 15123531]
38. Grobner T. Gadolinium--a specific trigger for the development of nephrogenic fibrosing dermopathy and nephrogenic systemic fibrosis? Nephrol Dial Transplant. 2006; 21:1104–1108. [PubMed: 16431890]

39. Marckmann P, Skov L, Rossen K, Dupont A, Damholt MB, Heaf JG, Thomsen HS. Nephrogenic systemic fibrosis: Suspected causative role of gadodiamide used for contrast-enhanced magnetic resonance imaging. J Am Soc Nephrol. 2006; 17:2359–2362. [PubMed: 16885403]
40. Muthupillai R, Flamm SD, Wilson JM, Pettigrew RI, Dixon WT. Acute myocardial infarction: Tissue characterization with T1rho-weighted MR imaging--initial experience. Radiology. 2004; 232:606–610. [PubMed: 15215547]
41. Witschey WR, Zsido GA, Koomalsingh K, Kondo N, Minakawa M, Shuto T, McGarvey JR, Levack MM, Contijoch F, Pilla JJ, Gorman JH 3rd, Gorman RC. In vivo chronic myocardial infarction characterization by spin locked cardiovascular magnetic resonance. J Cardiovasc Magn Reson. 2012; 14:37. [PubMed: 22704222]
42. Goldfarb JW, Arnold S, Han J. Recent myocardial infarction: Assessment with unenhanced T1-weighted MR imaging. Radiology. 2007; 245:245–250. [PubMed: 17885192]
43. Dall'Armellina E, Ferreira VM, Kharbanda RK, Prendergast B, Piechnik SK, Robson MD, Jones M, Francis JM, Choudhury RP, Neubauer S. Diagnostic value of pre-contrast T1 mapping in acute and chronic myocardial infarction. JACC Cardiovasc Imaging. 2013; 6:739–742. [PubMed: 23764100]
44. Stanisz GJ, Odrobina EE, Pun J, Escaravage M, Graham SJ, Bronskill MJ, Henkelman RM. T1, T2 relaxation and magnetization transfer in tissue at 3T. Magn Reson Med. 2005; 54:507–512. [PubMed: 16086319]
45. Chen J, Song SK, Liu W, McLean M, Allen JS, Tan J, Wickline SA, Yu X. Remodeling of cardiac fiber structure after infarction in rats quantified with diffusion tensor MRI. Am J Physiol Heart Circ Physiol. 2003; 285:H946–954. [PubMed: 12763752]
46. Wu MT, Tseng WY, Su MY, Liu CP, Chiou KR, Wedeen VJ, Reese TG, Yang CF. Diffusion tensor magnetic resonance imaging mapping the fiber architecture remodeling in human myocardium after infarction: Correlation with viability and wall motion. Circulation. 2006; 114:1036–1045. [PubMed: 16940196]
47. Simpson JH, Carr HY. Diffusion and nuclear spin relaxation in water. The Physical Review. 1958; 111:1201–1202.
48. Robson MD, Piechnik SK, Tunnicliffe EM, Neubauer S. T1 measurements in the human myocardium: The effects of magnetization transfer on the SASHA and MOLLI sequences. Magn Reson Med. 2013; 70:664–670.
49. Scholz TD, Hoyt RF, DeLeonardis JR, Ceckler TL, Balaban RS. Water-macromolecular proton magnetization transfer in infarcted myocardium: A method to enhance magnetic resonance image contrast. Magn Reson Med. 1995; 33:178–184. [PubMed: 7707907]
50. Weber OM, Speier P, Scheffler K, Bieri O. Assessment of magnetization transfer effects in myocardial tissue using balanced steady-state free precession (bSSFP) cine MRI. Magn Reson Med. 2009; 62:699–705. [PubMed: 19572387]

NIH-PA Author Manuscript
NIH-PA Author Manuscript

Clinical Perspective

Prognostic outcome in patients with myocardial infarction (MI) is significantly determined by the location, size and transmurality of the MI. Over the past decade, Late Gadolinium Enhancement (LGE) Cardiac Magnetic Resonance Imaging (CMR) has evolved into a robust non-invasive imaging technique for detecting acute and chronic MI with excellent diagnostic accuracy. However, it is estimated that in nearly 20% of the acute MI population with comorbidity of late-stage chronic kidney disease, LGE CMR may be contraindicated. In this work we propose and test a contrast-agent-free CMR approach for characterizing chronic MIs using a canine model of infarction. We show that the proposed CMR approach has excellent diagnostic accuracy relative to LGE CMR. We anticipate that the proposed approach may be a compelling alternative to LGE CMR, especially in patients who are contraindicated for gadolinium but would otherwise benefit from infarct characterization.

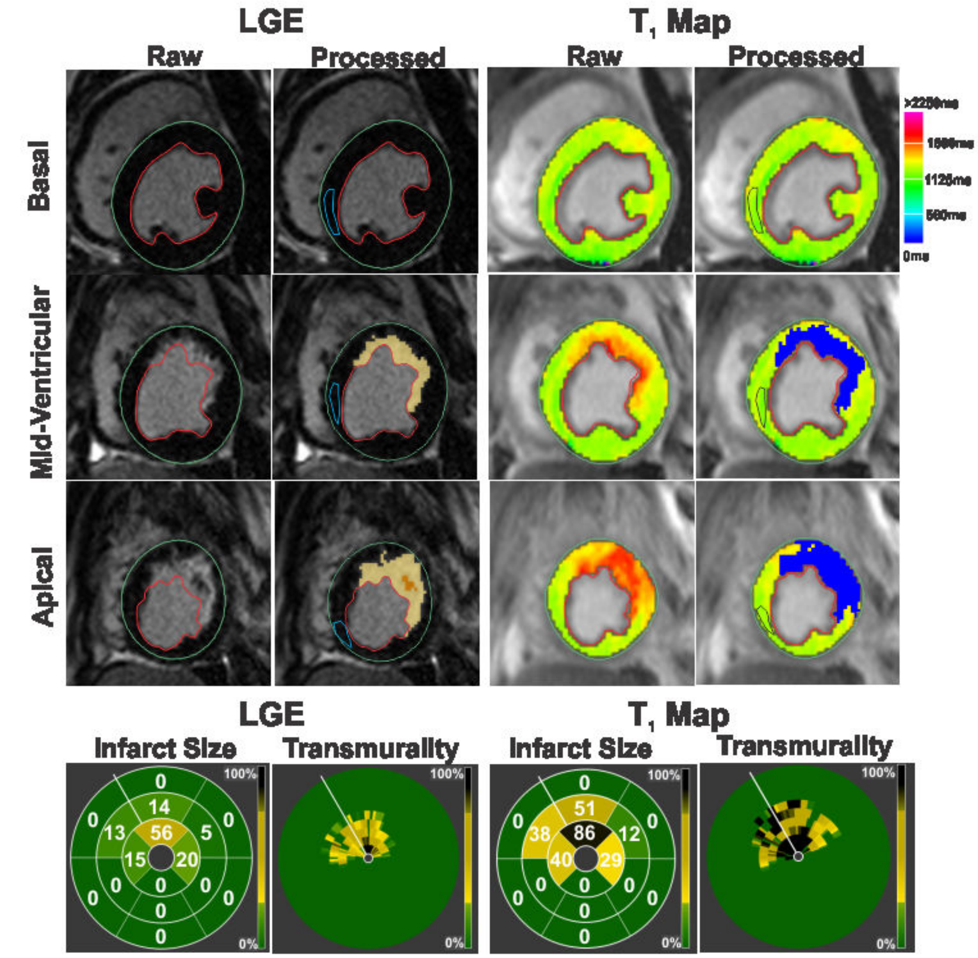

Figure 1. Detecting acute myocardial infarction at 3T

Representative LGE images and T_1 maps of basal, mid-ventricular and apical slices acquired at 7 days post MI from a canine scanned at 3T are shown. Infarcted myocardium (highlighted blue pixels in the processed images) was identified on both LGE images and T_1 maps using the mean+5SD criterion with respect to the reference ROI drawn in remote myocardium (blue contour). Bulls-eye plots depicting the extent and transmurality of the infarcted myocardium are also shown for both LGE images and T_1 maps. The number within each segment indicates the percentage volume of that segment that was detected as infarcted myocardium by the mean+5SD criterion. For transmurality, each slice was divided into 100 equally spaced chords with the first chord placed at the anterior insertion of the RV into the LV. Each concentric ring on the Bulls-eye plot represents each short-axis slice with the most basal slice represented by the outermost ring.

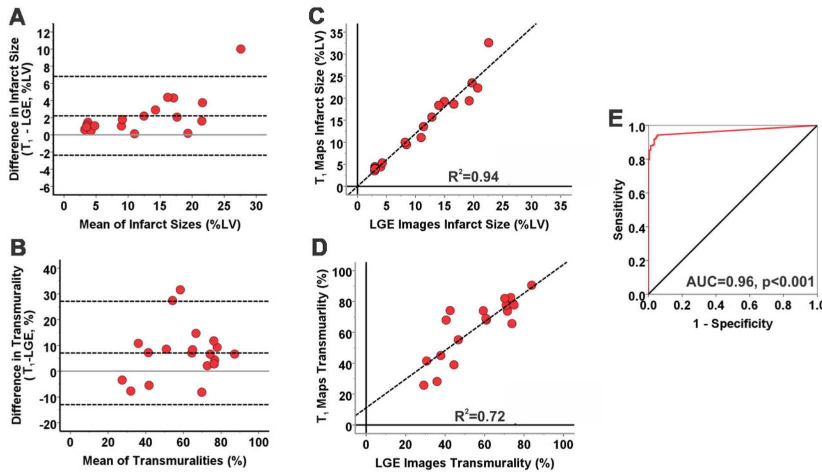

Figure 2. Diagnostic performance of native T_1 maps for detecting acute myocardial infarction at 3T

Bland-Altman analysis showed good agreement between LGE images and T_1 maps for measuring infarct size (A) and transmurality (B) in AMI at 3T. T_1 maps modestly overestimated infarct size and transmurality compared to LGE images. There were also strong correlations between LGE images and T_1 maps for measuring infarct size (R^2=0.94, C) and transmurality (R^2=0.72, D). ROC analysis showed that area under the curve was 0.96 (E) indicating a strong diagnostic performance of native T_1 maps for detecting AMI at 3T.

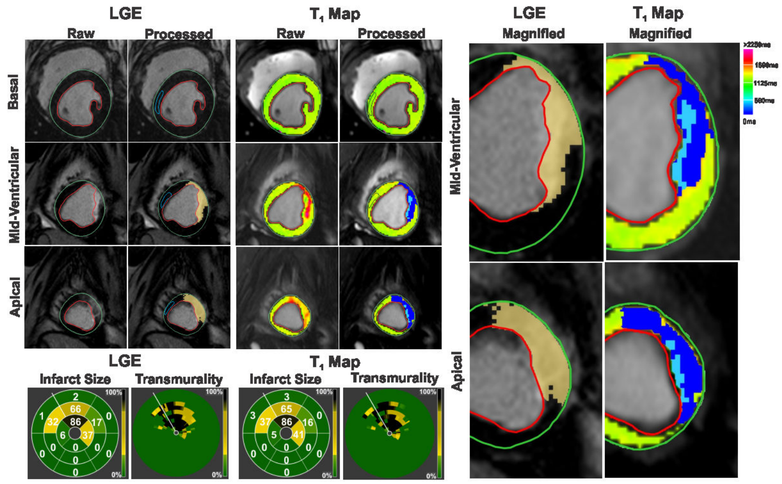

Figure 3. Detecting chronic myocardial infarction at 3T

Representative LGE images and T_1 maps of basal, mid-ventricular and apical slices acquired at 4 months post MI from a canine scanned at 3T are shown. Infarcted myocardium (highlighted dark blue pixels in the processed images) was identified on both LGE images and T_1 as in Figure 1. Hypointense core of chronic iron deposition within the hyperintense infarcted myocardium was not detected as infarcted myocardium by the mean+5SD criterion, and was manually included in the final analysis (highlighted light blue pixels in the processed images). Bulls-eye plots depicting the extent and transmurality of the infarcted myocardium are also shown for both LGE images and T_1 maps. Excellent correlations were observed between LGE images and T_1 maps in terms of the location, spatial extent and transmurality of the infarcted myocardium. Magnified views (on the right) of the infarcted myocardium detected on the mid-ventricular and apical slices clearly show the concordance between LGE images and T_1 maps.

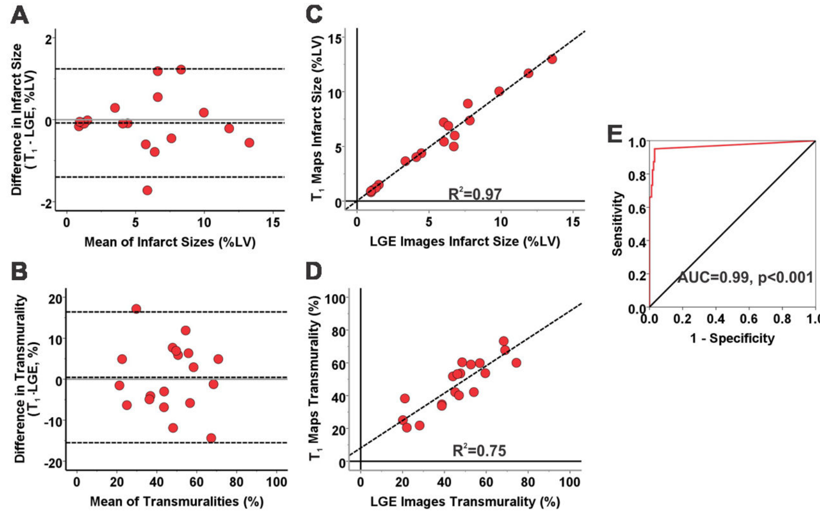

Figure 4. Diagnostic performance of native T_1 maps for detecting chronic myocardial infarction at 3T

Bland-Altman analysis showed excellent agreement between LGE images and T_1 maps for measuring infarct size (A) and transmurality (B) during the chronic phase at 3T. Excellent correlations were observed between LGE images and T_1 maps for measuring infarct size (R^2=0.97; C) and transmurality (R^2=0.75; D). ROC analysis showed that the area under the curve was 0.99 (E).

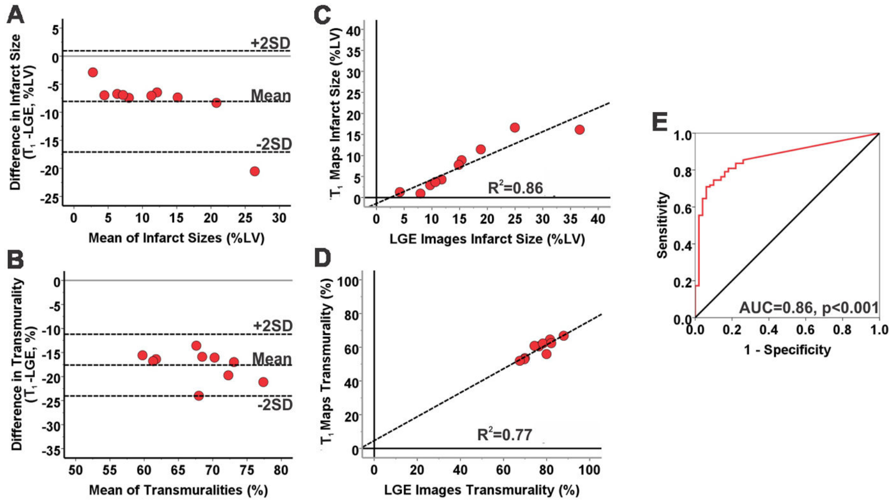

Figure 5. Diagnostic performance of native T_1 maps for detecting acute myocardial infarction at 1.5T

Bland-Altman analysis showed moderate agreement between LGE images and T_1 maps for measuring infarct size (A) and transmurality (B) using the mean + 5SD criterion at 1.5T in AMI. T_1 maps significantly underestimated infarct size and transmurality compared to LGE images. However, strong correlations were observed between LGE images and T_1 maps for measuring acute infarct size (R^2=0.86; C) and transmurality (R^2=0.77; D). ROC analysis showed that area under the curve was 0.86 (E).

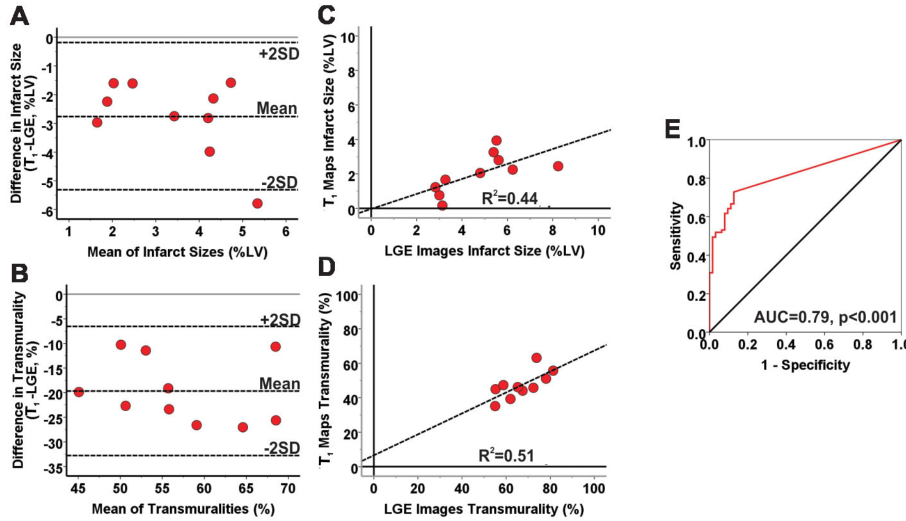

Figure 6. Diagnostic performance of native T_1 maps for detecting chronic myocardial infarction at 1.5T

Bland-Altman analysis showed poor agreement between LGE images and T_1 maps for measuring infarct size (A) and transmurality (B) during the chronic phase at 1.5T. T_1 maps greatly underestimated infarct size and transmurality compared to LGE images. Moderate correlations were observed between LGE images and T_1 maps for measuring infarct size (R^2=0.44; C) and transmurality (R^2=0.51; D). ROC analysis showed that area under the curve was 0.79 (E).

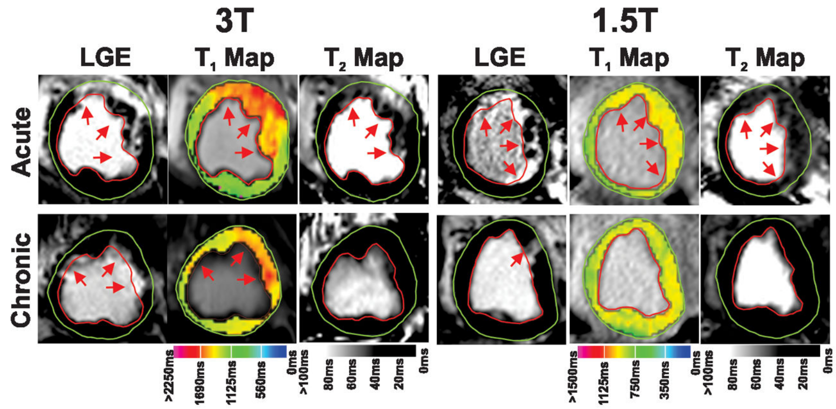

Figure 7.

T_1 and T_2 characteristics of infarcted myocardium at 1.5T and 3T during acute and chronic phases of infarction.

Representative LGE images, T_1 maps and T_2 maps acquired at 1.5T and 3T from four different canines at 7 days and 4 months post MI are shown. Arrows point to the hyperintense sites of LGE, T_1 and T_2. Significant T_1 and T_2 increases were visually evident within the infarcted territories in AMI at 3T. While T_1 elevations persisted at 4 months post MI at 3T, T_2 of the infarcted myocardium returned to baseline levels. At 1.5T, T_1 and T_2 of infarcted myocardium were significantly increased in AMI. However, both T_1 and T_2 values of the infarcted myocardium were not visually different from those of remote myocardium in CMI at 1.5T.

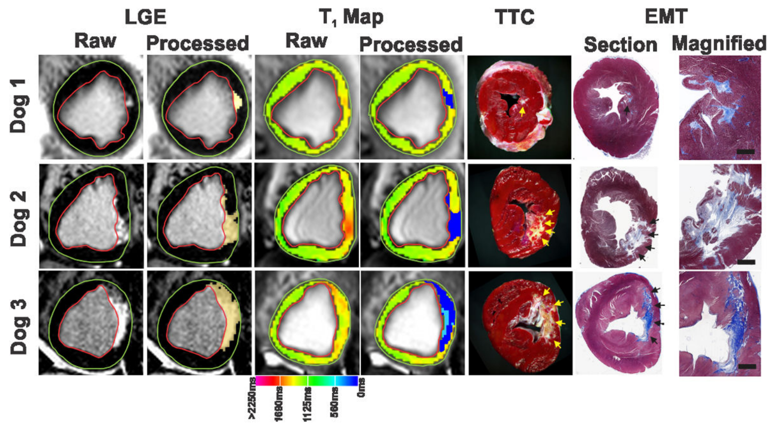

Figure 8. Histopathological validation of replacement fibrosis detected on LGE images and native T_1 maps during the chronic phase of MI at 3T

Representative LGE images and T_1 maps acquired from three different canines scanned at 3T at 4 months post MI are shown along with the corresponding ex-vivo slice-matched TTC and EMT-stained images. Highlighted blue pixels on the processed images show the site of infarction on LGE images and T_1 maps, while arrows point to the site of infarction in TTC and EMT images. Both LGE images and T_1 maps agreed well with ex-vivo TTC images in terms of spatial location of the infarcted myocardium. T_1 maps could reliably detect infarctions ranging in size from 1.2% of the total LV (Dog 1) to 12.9% of the total LV (Dog 3). Highlighted light blue pixels on the processed T_1 map from dog 3 point to the presence of chronic iron deposition. Corresponding to the chronic iron deposition seen on T_1 map, TTC image shows a yellow-brown discoloration in the necrotic core indicating the presence of iron. Additional histological validation using EMT staining confirmed extensive replacement fibrosis within the infarcted regions indicating that T_1 hyperintensity in the chronic phase of infarction at 3T predominantly arose from fibrosis. Scale bars on the magnified views of EMT images measure 2 mm.

NIH-PA Author Manuscript
NIH-PA Author Manuscript

Table 1

Typical imaging parameters used to acquire different CMR images at 1.5T and 3T

Imaging Method	Cine		Native T_1 map		Native T_2 map		LGE	
Field Strength	3T	1.5T	3T	1.5T	3T	1.5T	3T	1.5T
Sequence	Balanced SSFP		Modified Look-Locker Inversion Recovery		T_2 – prepared SSFP		IR – prepared GRE	
TR/TE (ms)	3.2/1.6	3.5/1.75	2.2/1.1	2.4/1.2	2.8/1.4	2.2/1.1	3.0/1.5	3.5/1.75
Flip Angle	50°	70°	35°		50°	70°	25°	40°
Bandwidth (Hz/pixel)	1371	930	1042	1002	1371	1002	586	1002
In-plane Resolution	1.3×1.3 mm^2							
Slice Thickness	6mm							
Other Parameters	25–30 cardiac phases		8 TIs; 2 inversion blocks of 3+5 images; minimum TI = 110ms; TI increment = 80ms		T_2-preparation times of 0, 24 and 55ms		Optimal TI to null the remote myocardium	

NIH-PA Author Manuscript
NIH-PA Author Manuscript

Table 2

T_1, T_2 and LGE signal intensity characteristics of acute and chronic myocardial infarction at 1.5T and 3T

Field Strength	**3T**				**1.5T**			
Time post MI	Day 7		Month 4		Day 7		Month 4	
Tissue Type	Remote	Infarcted	Remote	Infarcted	Remote	Infarcted	Remote	Infarcted
Native T_1 (ms)	1230±63	1563±154	1257±138	1485±139	924±72	1104±108	976±80	1060±116
Native ΔT_1 between Remote and Infarcted Myocardium (ms)	329± 119		239±104		184±77		89±38	
T_2 (ms)	46±4	64±9	44±4	46±3	50±4	69±5	49±5	51±6
ΔT_2 between Remote and Infarcted Myocardium (ms)	18±6		2±3		19±7		2±5	
%Change in Native T_1 with respect to Remote	26±8		19±7		14±8		12±6	
%Change in LGE signal intensity with respect to Remote	728±484		790±513		376±192		409±163	
Sensitivity of Native T_1 Maps	94%		95%		84%		58%	
Specificity of Native T_1 Maps	94%		97%		74%		78%	